

A Technique for Improving the Accuracy of Finite Element Solutions for Magnetotelluric Data

William L. Rodi

(Received 1975 July 11)*

Summary

This paper develops a finite element method which gives accurate numerical approximations to magnetotelluric data over two-dimensional conductivity structures. The method employs a simple finite element technique to find the field component parallel to the strike of the structure and a new numerical differentiation scheme to find the field component perpendicular to strike. Examples show that the new numerical differentiation scheme is a significant improvement over the standard finite element procedure when meshes of poor quality are used. Algorithms for incorporating the differentiation scheme into the finite element matrix equation and for computing partial derivatives of magnetotelluric data with respect to mesh parameters are derived in order to simplify the computation needed to do the inverse problem.

1. Introduction

The magnetotelluric (MT) response over an arbitrary two-dimensional conductivity structure can only be solved with numerical methods such as finite element (FE) and finite difference. In the usual application of these methods, the component of the electric or magnetic field parallel to the strike of the structure (E_x or H_x) is found approximately at a finite number of points (or nodes) that describe a mesh. Values of this 'solution field' between nodes can be estimated by interpolation. The field components not found directly, 'auxiliary fields', can also be estimated—typically by numerical differentiation of the solution field.

For a given problem and mesh, the degree to which the numerical solution, as parameterized by the mesh, can describe the spatial variations of the analytical solution determines the quality of the mesh. In general, mesh quality increases with the number of nodes used, but considerations of computer time and size of computer memory place a practical upper limit on this number. Also, the accuracy of the solution fields is usually greater than the accuracy of the auxiliary fields. One possible way to handle this problem is to numerically solve the first order Maxwell's equations for all the field components directly. This raises the status of the auxiliary fields to that of solution fields and avoids numerical differentiation. This multi-component approach, however, is very time and memory demanding. Given the one-component approach (two-component if E_x and H_x do not decouple into independent modes), the accuracy of numerical methods is dictated by the practical limits on mesh quality and the technique used to compute auxiliary fields.

* Received in original form 1975 February 4

In spite of these limitations, several published numerical schemes (for example, Swift 1967; Coggon 1971; Jones & Pascoe 1971; Pascoe & Jones 1972) give accurate results for electromagnetic problems provided each mesh used is carefully designed to suit the conductivity structure and frequency. One important consideration in mesh design is to avoid very non-uniform node spacing. This was illustrated by Williamson, Hewlett & Tammemagi (1974) with regard to the Jones & Pascoe (1971), Pascoe & Jones (1972) finite difference method and confirmed by Jones & Thomson (1974). Another consideration is the problem of having a too large vertical node spacing near the Earth's surface, which results in an inaccurate estimate of the auxiliary fields E_y and H_y , obtained by differentiating with respect to depth. Pascoe & Jones (1972) improve the accuracy of E_y and H_y by assuming that E_x and H_x have the analytic one-dimensional functional dependence on depth (exponentials) between nodes. As pointed out by the authors, it is not clear that this procedure is appropriate for the general two-dimensional problem.

The purpose of this paper is to present an implementation of the FE method that gives accurate solution fields and auxiliary fields in situations where good mesh design is not easy to accomplish. One such situation occurs when there are large lateral changes in electrical conductivity. For example, if a vertical contact separates a 100 : 1 conductivity contrast, then a vertical node spacing equal to 0.02 skin depths (a more than adequate spacing) on the resistive side of the contact is equal to 0.2 skin depths (a marginally adequate spacing) on the conductive side. To get adequate node spacing everywhere would require either the addition of many nodes to the mesh, the use of very uneven node spacing, or the use of a general FE mesh that allows arbitrary placement of nodes.

A second example of mesh design problems occurs in the application of linear inverse methods to MT data interpretation. The methods of Backus & Gilbert (1967) and Jordan (1973) for iteratively improving an Earth model require the solution of many forward problems—one per datum per iteration. Partial derivatives of each datum with respect to all the model parameters must also be computed for each iteration. Therefore, two difficulties with numerical methods are aggravated. First, since so many forward problems are solved and partial derivative calculations are necessary, limits on the number of nodes used are severe. Second, the mesh cannot be designed carefully except for the initial guess model. Each change to the conductivity structure makes the mesh less suitable for the next iteration. The mesh can be changed iteratively, but writing a successful algorithm for improving the mesh at each step of the iteration would be difficult.

The numerical scheme described in this paper reduces some of the harmful effects of bad mesh design. This is achieved with a new technique for numerically differentiating the solution field to get the auxiliary field needed to define MT apparent conductivity. The solution field is obtained with a simple FE scheme that leads to a matrix equation very similar to the transmission network equations given by Swift (1967). The equation can be solved by the same upper-triangularization and back-substitution algorithm used by Swift. More versatile applications of the FE method to electromagnetic problems, using general mesh geometries and a general parameterization of the solution field, are described by Reddy & Rankin (1973), Silvester & Haslam (1972) and Coggon (1971). The numerical differentiation technique developed in this paper could also be developed for these or other FE methods. The technique developed here might also be used as an alternative to more elaborate methods.

2. The magnetotelluric equations

If electrical conductivity σ , magnetic permeability μ , and electric permittivity ϵ are independent of the x co-ordinate (see Fig. 1), then two uncoupled electro-

magnetic modes exist when sources and boundary conditions are also independent of x . The ' H_x mode' involves the field components H_x , E_y , and E_z ; the ' E_x mode' involves E_x , H_y , and H_z . Following Swift (1967), Maxwell's equations for both modes can be written (assuming $e^{-i\omega t}$ time-dependence and mks units)

$$\left. \begin{aligned} \partial_y I + \partial_z J &= -\gamma V \\ \partial_z V &= -\eta J \\ \partial_y V &= -\eta I \end{aligned} \right\} \quad (2.1)$$

using the following substitutions:

	H_x mode	E_x mode
$V =$	H_x	E_x
$J =$	$-E_y$	H_y
$I =$	E_z	$-H_z$
$\eta =$	$\sigma - i\omega\epsilon$	$-i\omega\mu$
$\gamma =$	$-i\omega\mu$	$\sigma - i\omega\epsilon$

The quantities H_x , μH_y , H_z , E_x , $(\sigma - i\omega\epsilon) E_y$, and E_z are continuous across a vertical contact that gives a discontinuity in σ , μ , or ϵ . H_x , H_y , μH_z , E_x , E_y , and $(\sigma - i\omega\epsilon) E_z$ are continuous across a horizontal contact. These continuity conditions can be summarized with

$V, I, \eta J$ continuous across vertical contacts

$V, \eta I, J$ continuous across horizontal contacts

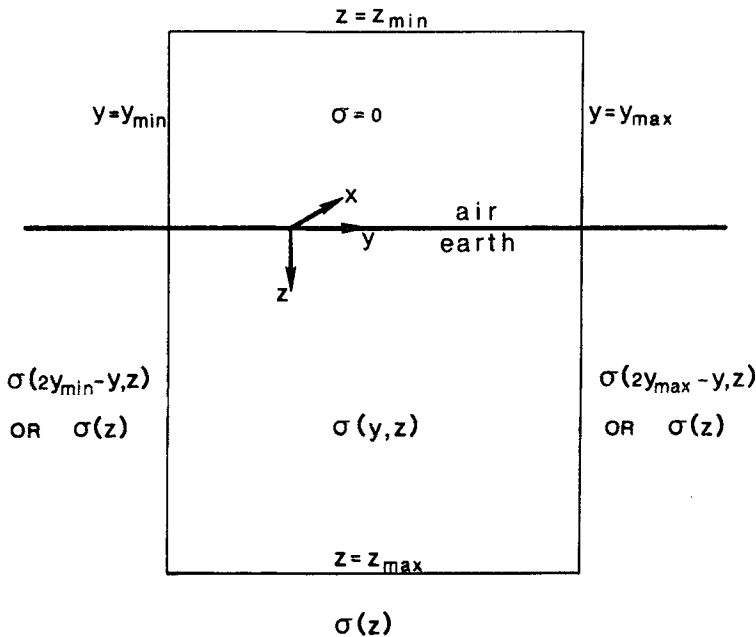


FIG. 1. Cross-section of a two-dimensional Earth model. Electrical parameters σ , μ , and ϵ depend on y and z inside the four boundaries. Outside the boundaries the parameters are either one-dimensional or symmetric about the lines $y = y_{min}$ and $y = y_{max}$.

One second order equation for V can be obtained from the three first order equations:

$$\partial_y((1/\eta)\partial_y V) + \partial_z((1/\eta)\partial_z V) = \gamma V. \quad (2.2)$$

The MT impedance for the two modes is defined to be

$$Z = \begin{array}{cc} H_x \text{ mode} & E_x \text{ mode} \\ \frac{-E_y}{H_x} = \frac{J}{V} & \frac{E_x}{H_y} = \frac{V}{J} \end{array}$$

and the complex apparent conductivity is $\sigma_A = -i\omega\mu/Z^2$. An MT datum is taken here to be either $\log_{10}|\sigma_A|$ or $\text{ph } \sigma_A$ (in degrees) at the radial frequency ω at a station on the Earth's surface.

Boundary conditions

The boundary conditions used in this paper simulate a plane wave source having no x or y dependence radiating above a halfspace which has electrical parameters $\sigma(y, z)$ and $\mu(y, z)^*$ inside a region $0 \leq z \leq z_{\max}$, $y_{\min} \leq y \leq y_{\max}$. In air ($z < 0$) $\sigma = 0$ and $\mu = 4\pi \times 10^{-7}$ (the free space value in mks units). Both σ and μ depend only on depth for $z > z_{\max}$.

The boundary conditions are specified at $y = y_{\max}$, $y = y_{\min}$, $z = z_{\max}$, and $z = z_{\min}$. The plane wave source is expressed by setting the horizontal magnetic field, H_x or H_y , to 1 at $z = z_{\min}$. In the H_x mode, $z_{\min} = 0$ because H_x is constant in air, as seen by setting $\eta = 0$ in (2.1). In the E_x mode, z_{\min} is negative and chosen such that the secondary fields induced by lateral changes in σ and μ are approximately zero at $z = z_{\min}$. If the boundary conditions described below are used at y_{\min} and y_{\max} , then choosing $z_{\min} < y_{\min} - y_{\max}$ is adequate for most realistic-Earth problems.

For both modes, z_{\max} must be large enough so that below z_{\max} either the secondary or total E_x or H_x field is negligibly small.

The y_{\min} and y_{\max} boundaries can be used to model two situations, which are illustrated in Fig. 1. First, if σ and μ depend only on depth outside $y_{\min} \leq y \leq y_{\max}$, then *approximate* boundary conditions can be imposed at $y = y_{\min}$ and $y = y_{\max}$ that express this. The approximation will be accurate if the boundaries are far from lateral changes in σ and μ , thus making the fields outside the boundaries essentially one-dimensional. The second situation permits the statement of *exact* boundary conditions. Namely, if σ and μ are symmetric about the lines $y = y_{\min}$ and $y = y_{\max}$ (and consequently periodic with a period of $2[y_{\max} - y_{\min}]$), then imposing $\partial_y E_x = 0$ or $\partial_y H_x = 0$ on the boundaries expresses this symmetry. Looking ahead to Section 8, both situations occur in the conductivity structure in Fig. 4. The structure is a 1 km square dyke underlain by an infinite conductor. The right-hand boundary is placed far from the dyke since the fields are approximately one-dimensional there. The left-hand boundary is placed at the centre of the dyke because this is a line of symmetry in the conductivity structure and in the fields.

The four boundary conditions can be expressed in the general form

$$z = z_{\max} \quad (1/\eta)\partial_z V + \alpha_1 V = \beta_1 \quad (2.3a)$$

$$z = z_{\min} \quad (1/\eta)\partial_z V + \alpha_2 V = \beta_2 \quad (2.3b)$$

$$y = y_{\max} \quad (1/\eta)\partial_y V + \alpha_3 V = \beta_3 \quad (2.3c)$$

$$y = y_{\min} \quad (1/\eta)\partial_y V + \alpha_4 V = \beta_4. \quad (2.3d)$$

* Displacement currents are ignored in magnetotellurics due to the low frequencies used. Therefore, ϵ is assumed to be zero everywhere including in air.

The boundary conditions discussed above are obtained by setting $\alpha_3 = \beta_3 = \alpha_4 - \beta_4 = 0$ and

	H_x mode	E_x mode
$\alpha_1 =$	Z_{HS}	Z_{HS}^{-1}
$\beta_1 =$	0	0
$\alpha_2 =$	L	0
$\beta_2 =$	L	-1

where Z_{HS} is the MT impedance of the half space $z > z_{max}$ and where L is a very large number.

3. Variational approach

The field $V(y, z)$ satisfying (2.2) and (2.3) can be derived from a variational principle:* $V(y, z)$ minimizes a functional $\mathcal{L}(V, \partial_y V, \partial_z V)$ called the Lagrangian. The theory behind this is available in many textbooks (see Morse & Feshbach 1953, Chapter 3, for a complete and original development) so only a brief summary is presented here.

The Lagrangian is written as an integral of the Lagrange density L :

$$\mathcal{L} = \text{Re} \int_{y_{min}}^{y_{max}} dy \int_{z_{min}}^{z_{max}} dz L(V, \partial_y V, \partial_z V). \tag{3.1}$$

The real quantity \mathcal{L} is minimized when V satisfies the complex Euler–Lagrange equation

$$\partial_z \left[\frac{\partial L}{\partial(\partial_z V)} \right] + \partial_y \left[\frac{\partial L}{\partial(\partial_y V)} \right] = \frac{\partial L}{\partial V}. \tag{3.2}$$

The Lagrange density for V is given by

$$\mathcal{L} = \text{Re} \int dy \int dz \left[\frac{1}{2\eta} (\partial_z V)^2 + \frac{1}{2\eta} (\partial_y V)^2 + \frac{\gamma}{2} V^2 \right]. \tag{3.3}$$

The Lagrange density in (3.3) inserted into (3.2) gives (2.2). To avoid the use of complex quantities, one could derive the same result by using the real part of L in two real Euler–Lagrange equations—one equation for the real part of V and one for the imaginary part.

Boundary conditions

The boundary conditions in (2.3) can also be incorporated into the variational approach by adding an integral over each boundary to the Lagrangian. For each of the four boundaries the following integrals are added:

$$z = z_{max} \quad \mathcal{L}_1 = \text{Re} \int dy \left[\frac{\alpha_1}{2} V^2 - \beta_1 V \right] \tag{3.4a}$$

$$z = z_{min} \quad \mathcal{L}_2 = -\text{Re} \int dy \left[\frac{\alpha_2}{2} V^2 - \beta_2 V \right] \tag{3.4b}$$

$$y = y_{max} \quad \mathcal{L}_3 = \text{Re} \int dz \left[\frac{\alpha_3}{2} V^2 - \beta_3 V \right] \tag{3.4c}$$

* The variational principle used is an extension of Hamilton’s principle from time-dependent conservative systems to dissipative systems described in the frequency domain.

$$y = y_{\min} \quad \mathcal{L}_4 = -\text{Re} \int dz \left[\frac{\alpha_4}{2} V^2 - \beta_4 V \right]. \quad (3.4d)$$

Minimizing $\mathcal{L} + \mathcal{L}_1 + \mathcal{L}_2 + \mathcal{L}_3 + \mathcal{L}_4$ is equivalent to solving equations (2.2) and (2.3). This is proved in Appendix 6 of Zienkiewicz (1971).

4. Finite element solution

The FE method finds the function $V(y, z)$, chosen from a restricted set of functions, that minimizes the Lagrangian. The method is described in detail in Zienkiewicz (1971) and is described here only for the particular implementation used in this paper.

The region $z_{\min} \leq z \leq z_{\max}, y_{\min} \leq y \leq y_{\max}$ is divided up into rectangular elements, each having uniform η and γ . A node is defined at the corner of each rectangle. Inside a given element having width w and height h , $V(y, z)$ is assumed to be of the form

$$V(y, z) = c_0 + c_1 y + c_2 z + c_3 yz. \quad (4.1)$$

The constants c_i are uniquely determined by the values of V at the four nodes of the element. Therefore, for all the elements in a mesh having M rows of elements and

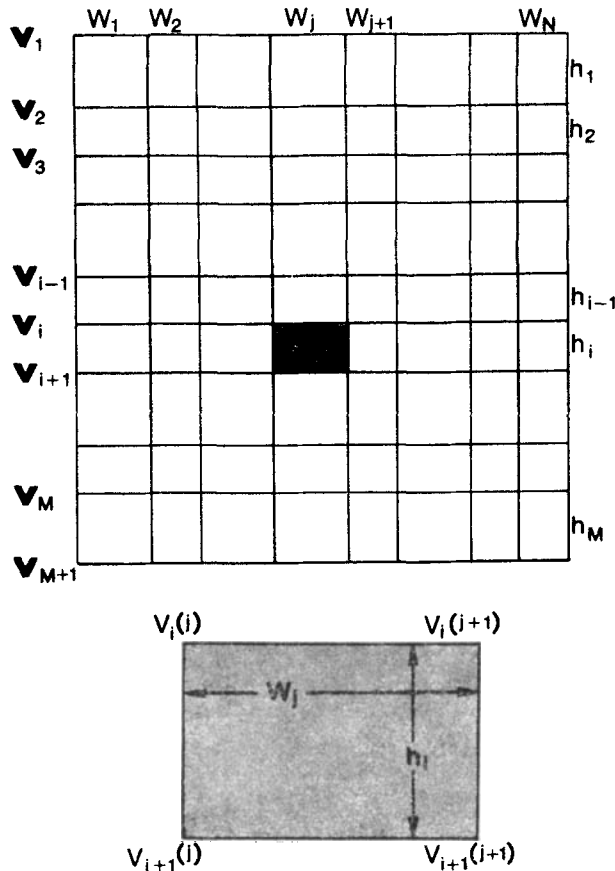


FIG. 2. Schematic diagram of a rectangular mesh. The vector v_i contains $N+1$ values of V along a row of nodes. The (i, j) th element, shaded and enlarged below, has mesh parameters $h_i, w_j, \eta_i(j)$, and $\gamma_i(j)$.

N columns of elements, the $(M+1)(N+1)$ values of V at the nodes determine $V(y, z)$ everywhere. This defines the set of functions from which the FE method chooses the one with the smallest Lagrangian. The parameterization of $V(y, z)$ with $(M+1)(N+1)$ values based on the functional form in (4.1) is the only approximation made in the FE method when the boundary conditions are exact.

The following notation, illustrated in Fig. 2, will be used to label the mesh parameters η, γ, h, w and the solution V . The values of V at the nodes immediately above the i 'th row of elements are denoted $V_i(j), j = 1, \dots, N+1$. In vector notation these values will be written as the $N+1$ by 1 column vector \mathbf{v}_i . Therefore \mathbf{v}_1 and \mathbf{v}_{M+1} are the vectors of values along the z_{\min} and z_{\max} boundaries respectively. The entire set of nodal values of V will be denoted by the $(M+1)(N+1)$ by 1 vector \mathbf{v} which consists of the \mathbf{v}_i placed end to end: $\mathbf{v} = (\mathbf{v}_1, \mathbf{v}_2, \dots, \mathbf{v}_{M+1})$. The element in the i 'th row and j 'th column of elements, the (i, j) 'th element, has parameters denoted $\eta_i(j), \gamma_i(j), h_i$ and w_j . Using these definitions, $V(y, z)$ inside element (i, j) can be written

$$\begin{aligned} V(y_j+y, z_i+z) = & V_i(j) \left[1 - \frac{y}{w_j} - \frac{z}{h_i} + \frac{yz}{w_j h_i} \right] \\ & + V_i(j+1) \left[\frac{y}{w_j} - \frac{yz}{w_j h_i} \right] \\ & + V_{i+1}(j) \left[\frac{z}{h_i} - \frac{yz}{w_j h_i} \right] + V_{i+1}(j+1) \left[\frac{yz}{w_j h_i} \right] \end{aligned} \quad (4.2)$$

where (y_j, z_i) is the location of the upper-left corner of the element.

The integrals in (3.3) and (3.4) can be expressed in terms of these quantities. \mathcal{L} in (3.3) is the sum of integrals over each element. The integral over element (i, j) is $\frac{1}{2} \mathbf{v}_e^T \mathbf{K}_e \mathbf{v}_e$ where \mathbf{v}_e is the 4 by 1 vector

$$\mathbf{v}_e = [V_i(j), V_i(j+1), V_{i+1}(j), V_{i+1}(j+1)]^T \quad (4.3)$$

and \mathbf{K}_e is the 4 by 4 symmetric (but not Hermitian) matrix

$$\mathbf{K}_e = \begin{bmatrix} K_1 & K_2 & K_3 & K_4 \\ K_2 & K_1 & K_4 & K_3 \\ K_3 & K_4 & K_1 & K_2 \\ K_4 & K_3 & K_2 & K_1 \end{bmatrix} \quad (4.4)$$

whose four independent components are

$$\begin{aligned} K_1 &= \frac{\gamma_i(j) h_i w_j}{9} + \frac{h_i}{3 w_j \eta_i(j)} + \frac{w_j}{3 h_i \eta_i(j)} \\ K_2 &= \frac{\gamma_i(j) h_i w_j}{18} - \frac{h_i}{3 w_j \eta_i(j)} + \frac{w_j}{6 h_i \eta_i(j)} \\ K_3 &= \frac{\gamma_i(j) h_i w_j}{18} + \frac{h_i}{6 w_j \eta_i(j)} - \frac{w_j}{3 h_i \eta_i(j)} \\ K_4 &= \frac{\gamma_i(j) h_i w_j}{36} - \frac{h_i}{6 w_j \eta_i(j)} - \frac{w_j}{6 h_i \eta_i(j)}. \end{aligned}$$

\mathbf{K}_e will be referred to as an element 'stiffness' matrix, a term borrowed from stress-strain analysis.

The integral of L over all of the elements can be assembled into one quadratic form involving all of the nodes: $\mathcal{L} = \text{Re} \frac{1}{2} \mathbf{v}^T \mathbf{K} \mathbf{v}$. \mathbf{K} is the $(M+1)(N+1)$ by $(M+1)(N+1)$ symmetric ‘global stiffness’ matrix whose components have contributions from each of the MN element stiffness matrices.

Boundary conditions

Adding the integrals in (3.4) to the Lagrangian expresses the boundary conditions. To derive the FE representation of \mathcal{L}_1 , assume the shaded element in Fig. 2 is on the z_{\max} boundary. If α_1 and β_1 are assumed to vary linearly along the bottom of the element, then they can be parameterized in terms of the node point values $\alpha_1(j)$, $\alpha_1(j+1)$, $\beta_1(j)$, and $\beta_1(j+1)$. Then (3.4a) integrated over the boundary of this one element contributes $\frac{1}{2} \mathbf{v}_e^T \mathbf{T}_e \mathbf{v}_e - \mathbf{v}_e^T \mathbf{f}_e$ to the Lagrangian where

$$\mathbf{T}_e = \begin{bmatrix} 0 & 0 & 0 & 0 \\ 0 & 0 & 0 & 0 \\ 0 & 0 & w_j [\frac{1}{4} \alpha_1(j) + \frac{1}{12} \alpha_1(j+1)] & w_j [\frac{1}{12} \alpha_1(j) + \frac{1}{2} \alpha_1(j+1)] \\ 0 & 0 & w_j [\frac{1}{12} \alpha_1(j) + \frac{1}{2} \alpha_1(j+1)] & w_j [\frac{1}{2} \alpha_1(j) + \frac{1}{4} \alpha_1(j+1)] \end{bmatrix} \quad (4.5)$$

and

$$\mathbf{f}_e = \left[0, 0, w_j \left(\frac{\beta_1(j)}{3} + \frac{\beta_1(j+1)}{6} \right), w_j \left(\frac{\beta_1(j)}{6} + \frac{\beta_1(j+1)}{3} \right) \right]^T. \quad (4.6)$$

It should be pointed out that the functions α_1 and β_1 are not necessarily continuous along the boundary. A discontinuity in η causes a discontinuity in α_1 and β_1 . Therefore, at each node on the boundary, two values of α_1 and β_1 are needed—one each for the elements to the left and right of the node. Thus in general, $2N$ nodal values of α and β are needed along the z_{\min} and z_{\max} boundaries.

The total integral in (3.4a) can be assembled from the element contributions. Similar contributions to (3.4b) through (3.4d) can be assembled from the other boundary elements. The total Lagrangian can then be written

$$\mathcal{L} + \mathcal{L}_1 + \mathcal{L}_2 + \mathcal{L}_3 + \mathcal{L}_4 = \text{Re} \{ \frac{1}{2} \mathbf{v}^T \mathbf{K} \mathbf{v} - \mathbf{v}^T \mathbf{f} \} \quad (4.7)$$

where \mathbf{K} includes the contributions from the \mathbf{T}_e and \mathbf{K}_e , and \mathbf{f} includes contributions from the \mathbf{f}_e . (4.7) is minimized when \mathbf{v} satisfies the complex matrix equation

$$\mathbf{K} \mathbf{v} = \mathbf{f}. \quad (4.8)$$

To avoid complex numbers, one could minimize (4.7) with respect to the real and imaginary parts of \mathbf{v} and derive a set of matrix equations which are just the real and imaginary parts of (4.8).

5. Computing J from V

In order to compute the MT impedance, V and J are needed at the Earth’s surface. V can be interpolated from the solution to (4.8) using (4.2). The standard FE procedure for computing J (defined to be $-(1/\eta) \partial_z V$) is to take the derivative of (4.2) and divide by η . Therefore, inside element (i, j) J has the form

$$J(y_j + y, z_i + z) = \frac{V_i(j) - V_{i+1}(j)}{h_i \eta_i(j)} \left[1 - \frac{y}{w_j} \right] + \frac{V_i(j+1) - V_{i+1}(j+1)}{h_i \eta_i(j)} \left[\frac{y}{w_j} \right]. \quad (5.1)$$

This formula is not very accurate unless h_i is very small. Computed this way, J is independent of z inside the element and is most accurate at $z = h_i/2$ and least accurate at the top and bottom of the element.

and node 2 is the first node below the surface, then from (5.2) and (5.3) J at the surface would be

$$J_1 = \frac{V_1 - V_2}{h_1 \eta_1}. \quad (5.10)$$

This is the standard FE definition of J for the one-dimensional case. The new method, (5.6) substituted into (5.3), gives

$$J_1 = \frac{V_1 - V_2}{h_1 \eta_1} + h_1 \gamma_1 \left(\frac{1}{3} V_1 + \frac{1}{6} V_2 \right). \quad (5.11)$$

The extra term in (5.11), not present in (5.10), corrects for the curvature of the solution field V . As an example of its effectiveness, (5.11) gives apparent conductivities to better than 0.5 per cent accuracy in one-dimensional problems in which (5.10) results in errors on the order of 15 per cent.

6. Partial derivatives with respect to mesh parameters

In order to apply linear inverse methods to MT data, partial derivatives of the data with respect to model parameters are needed. In FE solutions for the data, a model parameter can be any of the mesh parameters η , γ , h , or w . An algorithm for computing the exact partial derivative of the FE-computed data with respect to any mesh parameter is derived in this section. The algorithm is based upon a technique derived by Madden (1972) for computing the sensitivity of voltages to impedances in electrical networks.

The datum at a given station on the Earth's surface is defined as either $\log_{10} |\sigma_A|$ or $\text{ph } \sigma_A$. For the E_x mode $\sigma_A = -i\omega\mu(J/V)^2$ and

$$\log \sigma_A = \log (\mu\omega/i) + 2 \log J - 2 \log V.$$

The data are

$$\log_{10} |\sigma_A| = (1/\log_{10}) \text{Re} (\log \sigma_A) \quad (6.1a)$$

$$\text{ph } \sigma_A = (180/\pi) \text{Im} (\log \sigma_A). \quad (6.1b)$$

Equations (6.1) also apply to the H_x mode with

$$\log \sigma_A = \log (\mu\omega/i) + 2 \log V - 2 \log J.$$

The FE approximation to the data can be written generally as

$$d = \text{Re or Im} \{k_0 [\log k_1 + 2 \log (\mathbf{a}^T \mathbf{v}) - 2 \log (\mathbf{b}^T \mathbf{v})]\} \quad (6.2)$$

where \mathbf{a} and \mathbf{b} form the proper linear combinations of the solution vector \mathbf{v} to give V and J at the station. The partial derivative with respect to a mesh parameter m is

$$\frac{\partial d}{\partial m} = \text{Re or Im} \left\{ k_0 \left[\frac{1}{k_1} \frac{\partial k_1}{\partial m} + \frac{2}{\mathbf{a}^T \mathbf{v}} \frac{\partial}{\partial m} (\mathbf{a}^T \mathbf{v}) - \frac{2}{\mathbf{b}^T \mathbf{v}} \frac{\partial}{\partial m} (\mathbf{b}^T \mathbf{v}) \right] \right\}. \quad (6.3)$$

The following derivation shows how to find $\partial Q/\partial m$ when Q has the form, $Q = \mathbf{a}^T \mathbf{v}$. Q can be either V or J .

First, note that the derivative of a matrix or a vector is gotten from component-by-component differentiation. Second, note that the quantities $\partial \mathbf{a}/\partial m$, $\partial \mathbf{f}/\partial m$, and $\partial \mathbf{K}/\partial m$ are known since \mathbf{a} , \mathbf{f} , and \mathbf{K} are given. To begin,

$$\frac{\partial Q}{\partial m} = \left(\frac{\partial \mathbf{a}}{\partial m} \right)^T \mathbf{v} + \mathbf{a}^T \left(\frac{\partial \mathbf{v}}{\partial m} \right). \quad (6.4)$$

Differentiating (4.8) gives

$$\frac{\partial \mathbf{K}}{\partial m} \mathbf{v} + \mathbf{K} \frac{\partial \mathbf{v}}{\partial m} = \frac{\partial \mathbf{f}}{\partial m}. \quad (6.5)$$

Equation (6.5) can be solved for $\partial \mathbf{v}/\partial m$ and substituted into (6.4) to yield

$$\frac{\partial Q}{\partial m} = \frac{\partial \mathbf{a}^T}{\partial m} \mathbf{v} + \mathbf{a}^T \mathbf{K}^{-1} \left(\frac{\partial \mathbf{f}}{\partial m} - \frac{\partial \mathbf{K}}{\partial m} \mathbf{v} \right). \quad (6.6)$$

This can be formulated as the following algorithm:

1. Solve for \mathbf{v} .
2. For each mesh parameter m ,
 - (a) Generate $\mathbf{x} = \partial \mathbf{f}/\partial m - (\partial \mathbf{K}/\partial m) \mathbf{v}$.
 - (b) Solve for \mathbf{y} in the problem $\mathbf{K} \mathbf{y} = \mathbf{x}$.
 - (c) For each \mathbf{a} ,
 - (i) Compute $(\partial \mathbf{a}/\partial m)^T \mathbf{v} + \mathbf{a}^T \mathbf{y}$.

This algorithm requires solving a forward problem, $\mathbf{K} \mathbf{y} = \mathbf{x}$, for each mesh parameter. So the algorithm is suitable for obtaining the derivatives for the data at several stations with respect to a few mesh parameters.

A more efficient algorithm is available when the derivatives of a few data with respect to many mesh parameters are wanted—namely, when the number of m 's exceeds the number of Q 's. In this algorithm one forward problem is done for each Q and is defined to be

$$\mathbf{K} \mathbf{u} = \mathbf{a} \quad (6.7)$$

which gives $\mathbf{u} = \mathbf{K}^{-1} \mathbf{a}$. Since \mathbf{K} is symmetric,

$$\mathbf{a}^T \mathbf{K}^{-1} \mathbf{x} = \mathbf{x}^T \mathbf{K}^{-1} \mathbf{a} = \mathbf{x}^T \mathbf{u} = \mathbf{u}^T \mathbf{x}. \quad (6.8)$$

Now (6.6) can be rewritten as

$$\frac{\partial Q}{\partial m} = \frac{\partial \mathbf{a}^T}{\partial m} \mathbf{v} + \mathbf{u}^T \left(\frac{\partial \mathbf{f}}{\partial m} - \frac{\partial \mathbf{K}}{\partial m} \mathbf{v} \right). \quad (6.9)$$

The algorithm is now

1. Solve for \mathbf{v} .
2. For each \mathbf{a} ,
 - (a) Solve for \mathbf{u} in the problem $\mathbf{K} \mathbf{u} = \mathbf{a}$.
 - (b) For each m ,
 - (i) Generate $\mathbf{x} = \partial \mathbf{f}/\partial m - (\partial \mathbf{K}/\partial m) \mathbf{v}$.
 - (ii) Compute $(\partial \mathbf{a}/\partial m)^T \mathbf{v} + \mathbf{u}^T \mathbf{x}$.

to the stiffness matrix required by MOM's method are easy to handle—one simply inserts two fictitious rows of elements in the mesh: one has $A_i = 0$, $B_i = M_i$ and the other has $A_i = 0$, $B_i = -M_i$. The algorithms for generating K and $\partial K/\partial m$ and for solving $Kv = f$ are unchanged by MOM's method.

The H_x mode is treated in a similar way. The Earth's surface is the z_{min} boundary on which V is set equal to 1. For a given station on the surface, V and J are computed from v_1 and g_1^+ . The original set of equations is

$$\begin{bmatrix} A_1 + T_1 & B_1 & & & \\ & B_1 & A_1 + A_2 & B_2 & \\ & & B_2 & A_2 + A_3 & B_3 \\ & & & B_3 & \ddots \\ & & & & \ddots \end{bmatrix} \begin{bmatrix} v_1 \\ v_2 \\ v_3 \\ \vdots \end{bmatrix} = \begin{bmatrix} T_1 \mathbf{1} \\ 0 \\ 0 \\ \vdots \end{bmatrix} \quad (7.5)$$

T_1 is M_1 multiplied by a huge number, so the first block of (7.5) essentially states $M_1 v_1 = M_1 \mathbf{1}$. MOM's method adds g_1^+ as an unknown in a new set of equations:

$$\begin{bmatrix} 0 & -M_1 & & & \\ -M_1 & A_1 & B_1 & & \\ & B_1 & A_1 + A_2 & B_2 & \\ & & B_2 & A_2 + A_3 & B_3 \\ & & & B_3 & \ddots \end{bmatrix} \begin{bmatrix} g_1^+ \\ v_1 \\ v_2 \\ v_3 \\ \vdots \end{bmatrix} = \begin{bmatrix} -M_1 \mathbf{1} \\ 0 \\ 0 \\ 0 \\ \vdots \end{bmatrix} \quad (7.6)$$

The first block in (7.6) expresses the boundary condition. The second block defines g_1^+ . Since the data stations are on the mesh boundary, the H_x mode requires only one extra vector of unknowns and one row of fictitious elements.

8. Examples

The examples in this section compare the accuracies of MT data computed two ways. The first way uses (5.2) and (5.3) to estimate J and is referred to as the 'standard' method. The second way uses MOM's method* for computing J based on the definitions in (5.6) and (5.3).

Three problems are solved: the H_x and E_x modes over the conductivity structure shown in Fig. 3 at a period of 100 s and the H_x mode over the conductivity structure in Fig. 4 with a period of 78 s. Both structures have $\epsilon = 0$ and $\mu = 4\pi \times 10^{-7}$ everywhere.

The following discussion examines the contribution MOM's method makes to the accuracy of FE solutions. To properly compare MOM's method to other published numerical results would require the addition of many examples to this section, so this comparison is not made. However, it is possible to state that for the vertical contact problem, the MOM data in Examples 1 and 3 compare favourably, allowing for differences in meshes, to the numerical results given in Tables 2 and 3 of Jones & Thomson (1974).

Example 1: H_x mode over vertical contact

The H_x mode response over a vertical contact with a conductivity contrast of 100 : 1 was solved using two FE meshes whose element dimensions are given in Table 1. Both meshes have 18 rows and 24 columns of elements, but Mesh 1.1 has grossly uneven node spacing. In both meshes the high conductivity region was terminated

* In this section and the next section the term MOM's method will, for convenience, be used to refer to both the algorithm derived in Section 7 and the new definition of J derived in Section 5 for which the algorithm is used.

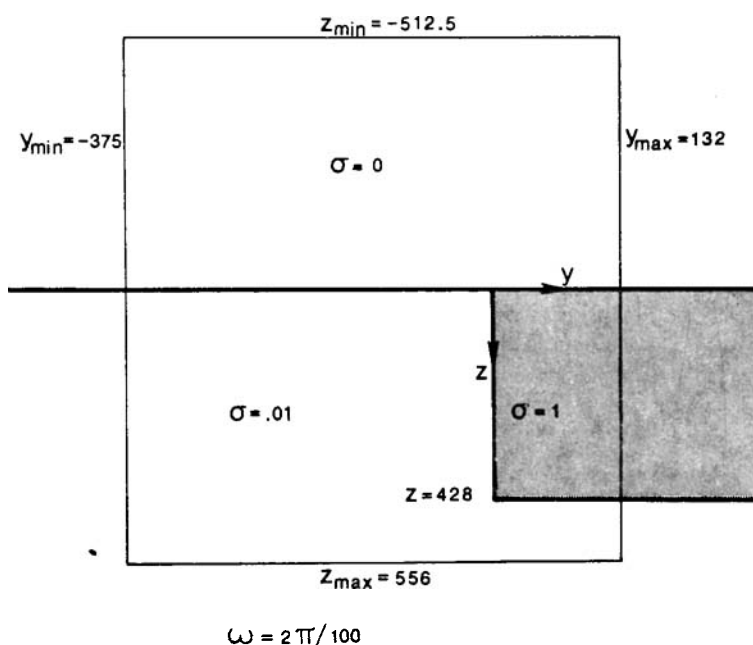


FIG. 3. Conductivity structure (not to scale) and frequency used for Examples 1 and 3. The thin lines indicate the mesh boundaries used for the FE solutions with the exception that $z_{\min} = 0$ in Example 1. Conductivities are in mho m^{-1} , distances in km, and frequency in rad s^{-1} .

at $z = 428$ km in order to accommodate the z_{\max} boundary condition, but this differs insignificantly from a semi-infinite vertical contact.

Table 2 compares five sets of MT data ($\log_{10} |\sigma_A|$ and $\text{ph } \sigma_A$) at selected points along the Earth's surface. The first column contains the analytic results of d'Erceville & Kunetz (1962) at the points where they tabulated the electric field. The remaining four columns of data were computed by the standard and MOM's methods using Meshes 1.1 and 1.2.

Inspection of Table 2 shows that for both meshes MOM's method is significantly more accurate than the standard method, especially on the conductive side of the contact where the skin depth is only 5 times h_1 . Also, it is apparent from comparing the Mesh 1.1 data to the Mesh 1.2 data that very irregular node spacing does not severely hamper either the standard or MOM implementation of the FE method.

Table 3 compares the standard and MOM's methods in a different way. The partial derivatives of each amplitude datum with respect to some element heights and widths are tabulated for the Mesh 1.1 solutions. Analytically these derivatives are zero since changing element dimensions does not move the position of the vertical contact.

In the FE solutions the partial derivatives will be non-zero for two reasons. First, changing element heights moves the conductivity contrast at $z = 428$ km and changing element widths moves the y_{\min} and y_{\max} boundaries (which changes the periodic conductivity structure). However, the mesh is so large, such perturbations of the conductivity model would have a slight effect on the data. Second, and most important, changing the h_i and w_j affect the data because of the FE approximation; moving nodes reparameterizes the solution field. This artificial dependence of the data on the mesh parameters results in the non-zero partial derivatives in Table 3. Comparison of the derivatives for the two methods shows that MOM's method does not reduce

Table 1

Element heights (h_i) and widths (w_j) in km for Meshes 1.1 and 1.2 used in Example 1. The word 'contact' appears when rows or columns of elements are separated by a conductivity contrast.

Mesh 1.1							
i	h_i	i	h_i	i	h_i	i	h_i
1	1.0	6	2.0	11	16.0	16	128.0
2	2.0	7	4.0	12	8.0	17	128.0
3	1.0	8	8.0	13	16.0	contact	
4	2.0	9	4.0	14	32.0	18	128.0
5	4.0	10	8.0	15	64.0		

j	w_j	j	w_j	j	w_j	j	w_j
1	160.0	8	5.0	13	0.5	19	2.0
2	80.0	9	10.0	14	1.0	20	4.0
3	40.0	10	5.0	15	0.5	21	8.0
4	20.0	11	10.0	16	1.0	22	16.0
5	10.0	12	5.0	17	2.0	23	32.0
6	20.0	contact		18	1.0	24	64.0
7	10.0						

Mesh 1.2							
i	h_i	i	h_i	i	h_i	i	h_i
1	1.0	6	3.4	11	10.4	16	128.0
2	1.3	7	4.0	12	13.6	17	128.0
3	1.7	8	5.2	13	16.0	contact	
4	2.0	9	6.8	14	32.0	18	128.0
5	2.6	10	8.0	15	64.0		

j	w_j	j	w_j	j	w_j	j	w_j
1	160.0	8	8.0	13	0.3	19	2.7
2	80.0	9	6.0	14	0.4	20	4.0
3	40.0	10	4.0	15	0.6	21	8.0
4	28.0	11	3.0	16	0.8	22	16.0
5	20.0	contact		17	1.2	23	32.0
6	15.0	12	0.2	18	1.8	24	64.0
7	11.0						

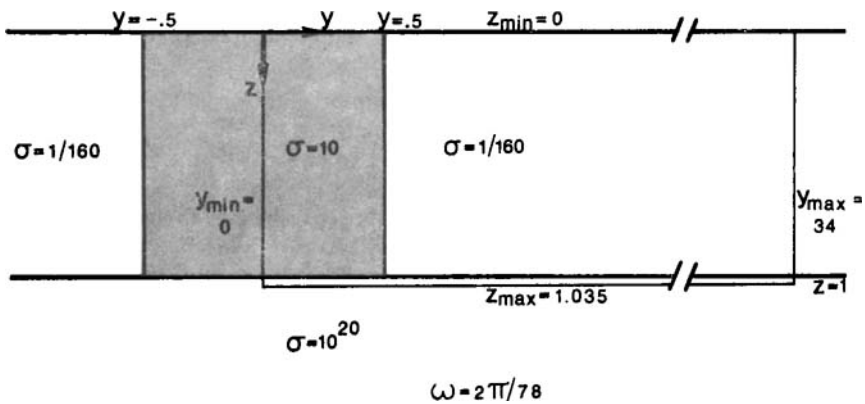


FIG. 4. Conductivity structure used in Example 2. The thin lines indicate mesh boundaries. Conductivities are in mho m^{-1} , distances in km, and frequency in rad s^{-1} .

Table 2

Comparison of amplitude and phase data for Example 1. 'd'E & K' refers to analytic results of d'Ereuveille & Kumetz (1962). 'Std' refers to standard FE definition of E_y . The difference between each datum and 'd'E & K' is in parentheses.

y (km)	Log ₁₀ Amplitude				Phase (degrees)
	d'E & K	Mesh 1.1 MOM	Mesh 1.1 Std	Mesh 1.2 MOM	
-375		-2.001	-1.992	-2.001	-1.992
-7.118	-2.047	-2.048 (-0.001)	-2.040 (0.007)	-2.046 (0.001)	-2.038 (0.009)
-3.559	-2.071	-2.075 (-0.004)	-2.066 (0.005)	-2.071 (0.0)	-2.063 (0.008)
-2.135	-2.087	-2.093 (-0.006)	-2.089 (-0.003)	-2.089 (-0.004)	-2.081 (0.006)
-1.424	-2.097	-2.102 (-0.005)	-2.093 (0.004)	-2.101 (-0.004)	-2.093 (0.004)
-0.712	-2.110	-2.112 (-0.002)	-2.102 (0.008)	-2.113 (-0.003)	-2.104 (0.006)
-0.356	-2.119	-2.116 (0.003)	-2.107 (0.012)	-2.119 (0.0)	-2.110 (0.009)
0.0	-2.133	-2.121 (0.012)	-2.111 (0.022)	-2.125 (0.008)	-2.115 (0.018)
+0.0	1.867	1.879 (0.012)	1.889 (0.022)	1.875 (0.008)	1.885 (0.018)
0.356	0.996	0.996	1.237	0.942	1.230
0.712	0.705	0.686 (-0.019)	0.924 (0.219)	0.696 (-0.009)	0.911 (0.206)
1.424	0.417	0.411 (-0.006)	0.572 (0.155)	0.409 (-0.008)	0.575 (0.158)
2.135	0.263	0.253 (-0.010)	0.394 (0.131)	0.259 (-0.004)	0.399 (0.136)
3.559	0.103	0.106 (0.003)	0.221 (0.118)	0.097 (-0.006)	0.212 (0.109)
7.118	-0.017	-0.020 (-0.003)	0.072 (0.089)	-0.016 (0.001)	0.075 (0.092)
132		-0.004	0.082	-0.003	0.083
-375		0.0	-1.2	-0.1	-1.2
-7.118	-3.5	-3.6 (-0.1)	-4.7 (-1.2)	-3.6 (-0.1)	-4.7 (-1.2)
-3.559	-3.3	-3.0 (0.3)	-4.2 (-0.9)	-3.5 (-0.2)	-4.5 (-1.2)
-2.135	-2.9	-2.4 (0.5)	-3.5 (-0.6)	-2.7 (0.2)	-3.9 (-1.0)
-1.424	-2.5	-2.0 (0.5)	-3.2 (-0.7)	-2.2 (0.3)	-3.3 (-0.8)
-0.712	-1.8	-1.7 (0.1)	-2.9 (-1.1)	-1.6 (0.2)	-2.8 (-1.0)
-0.356	-1.2	-1.5 (-0.3)	-2.8 (-1.6)	-1.3 (-0.1)	-2.6 (-1.4)
0.0	0.0	-1.4 (-1.4)	-2.6 (-2.6)	-1.1 (-1.1)	-2.3 (-2.3)
+0.0	0.0	-1.4 (-1.4)	-2.6 (-2.6)	-1.1 (-1.1)	-2.3 (-2.3)
0.356	41.7	41.7	25.0	44.5	25.4
0.712	43.2	44.4 (1.2)	29.3 (-13.9)	43.5 (0.3)	29.8 (-13.4)
1.424	39.3	39.7 (0.4)	29.3 (-10.0)	39.7 (0.4)	28.9 (-10.4)
2.135	34.5	35.4 (0.9)	25.5 (-9.0)	34.9 (0.4)	24.9 (-9.6)
3.559	25.6	26.3 (0.7)	16.9 (-8.7)	26.0 (0.4)	16.6 (-9.0)
7.118	10.0	10.8 (0.8)	1.0 (-9.0)	10.7 (0.7)	0.9 (-9.1)
132		0.7	-10.2	0.5	-10.5

Table 3

Partial derivatives of $\log_{10} |\sigma_A|$ at 13 surface stations with respect to 10 of the mesh parameters of Mesh 1.1 in Example 1. Each station is located in the j 'th column of elements counting from left.

		Mesh 1.1 MOM									
y (km)	j	w_{12}	w_{13}	w_{14}	w_{15}	w_{16}	w_{17}	w_{18}	w_{19}	h_1	h_2
-7.118	11	0.0027	0.0002	0.0	0.0	0.0	0.0002	0.0	0.0	-0.0001	0.0002
-3.559	12	-0.0038	-0.0001	0.0	0.0001	0.0	-0.0002	0.0	-0.0001	0.0002	0.0003
-2.135	12	-0.0014	-0.0004	0.0	0.0001	0.0	-0.0003	0.0	-0.0001	0.0005	0.0003
-1.424	12	-0.0003	-0.0005	-0.0001	0.0001	0.0	-0.0003	0.0	-0.0001	0.0006	0.0004
-0.712	12	0.0009	-0.0006	-0.0002	0.0001	0.0	-0.0003	0.0	-0.0001	0.0008	0.0004
-0.356	12	0.0014	-0.0007	-0.0002	0.0001	0.0	-0.0003	0.0	-0.0001	0.0008	0.0004
0.0	12/13	0.0020	-0.0008	-0.0002	0.0001	0.0	-0.0003	0.0	-0.0001	0.0009	0.0004
0.356	13	0.0007	0.4506	0.0092	0.0025	-0.0001	-0.0009	0.0	-0.0001	-0.0684	-0.0039
0.712	14	0.0004	-0.1653	0.0238	0.0009	-0.0002	-0.0011	0.0	-0.0001	-0.0509	-0.0050
1.424	14	0.0002	0.0574	0.0527	-0.0033	-0.0005	-0.0016	0.0	-0.0002	0.0051	-0.0060
2.135	16	0.0001	-0.0274	-0.0299	-0.0269	0.0040	-0.0020	0.0	-0.0002	0.0027	-0.0058
3.559	17	0.0	-0.0154	-0.0165	-0.0155	-0.0168	0.0046	0.0001	-0.0003	0.0024	-0.0033
7.118	19	0.0	0.0010	0.0008	0.0010	0.0007	-0.0006	0.0007	0.0039	0.0017	0.0005
Mesh 1.1 Std											
-7.118	11	0.0026	0.0	0.0	0.0	0.0	-0.0002	0.0	0.0	-0.8608	0.0002
-3.559	12	-0.0036	0.0001	0.0	0.0001	0.0	-0.0002	0.0	-0.0001	-0.8599	0.0003
-2.135	12	-0.0014	-0.0001	-0.0001	0.0001	0.0	-0.0003	0.0	-0.0001	-0.8586	0.0004
-1.424	12	-0.0003	-0.0001	-0.0001	0.0001	0.0	-0.0003	0.0	-0.0001	-0.8582	0.0004
-0.712	12	0.0007	0.0001	-0.0001	0.0001	0.0	-0.0003	0.0	-0.0001	-0.8577	0.0004
-0.356	12	0.0012	-0.0001	-0.0001	0.0001	0.0	-0.0003	0.0	-0.0001	-0.8577	0.0004
0.0	12/13	0.0017	0.0001	-0.0001	0.0001	0.0	-0.0003	0.0	-0.0001	-0.8573	0.0004
0.356	13	0.0008	0.1360	-0.0068	0.0005	-0.0001	-0.0011	0.0	-0.0001	-0.7183	-0.0047
0.712	14	0.0004	-0.1114	0.0231	0.0007	-0.0002	-0.0014	0.0	-0.0002	-0.6996	-0.0064
1.424	14	0.0002	0.0812	0.0823	0.0009	-0.0003	-0.0018	0.0	-0.0002	-0.7105	-0.0077
2.135	16	0.0001	-0.0275	-0.0310	-0.0276	0.0042	-0.0022	0.0	-0.0003	-0.7296	-0.0064
3.559	17	0.0	-0.0181	-0.0181	-0.0172	-0.0185	0.0054	0.0001	-0.0003	-0.7531	-0.0031
7.118	19	0.0	0.0012	0.0010	0.0012	0.0009	-0.0004	0.0009	0.0045	-0.7761	0.0012

the artificial dependence on the element widths, but does greatly reduce the dependence on h_1 . This is because the standard method makes J a constant with depth inside each element while MOM's method allows a linear variation of J with depth.

Example 2: H_x mode over conductive dyke

The H_x mode over the conductivity model in Fig. 4 was solved analytically by Rankin (1962). These analytic results were not used in this example due to difficulties in tabulating the graphical presentation of the solution, but Rankin's solution does show that the problem is a challenging one. Instead, numerical solutions were computed for three meshes (see Table 4). Mesh 2.1 is very detailed and its data were taken to be very close to the true data; the value computed from Mesh 2.1 at $y = 34$ km, where the fields are one-dimensional, agrees well with the analytic value: $\log_{10} |\sigma_A| =$

Table 4

Element dimensions for Meshes 2.1, 2.2, and 2.3 used in Example 2.

Mesh 2.1							
i	h_i	i	h_i	i	h_i	i	h_i
1	0.01	8	0.03	15	0.1	20	0.002
2	0.01	9	0.05	16	0.1	21	0.003
3	0.015	10	0.05	17	0.08	22	0.004
4	0.015	11	0.06	18	0.07	23	0.006
5	0.02	12	0.08	19	0.05	24	0.008
6	0.03	13	0.1	contact		25	0.012
7	0.03	14	0.1				
j	w_j	j	w_j	j	w_j	j	w_j
1	0.04	13	0.02	25	0.002	36	0.17
2	0.03	14	0.02	contact		37	0.2
3	0.03	15	0.02	26	0.01	38	0.2
4	0.025	16	0.02	27	0.02	39	0.3
5	0.025	17	0.02	28	0.03	40	0.5
6	0.025	18	0.02	29	0.04	41	0.5
7	0.025	19	0.015	30	0.05	42	1.0
8	0.025	20	0.015	31	0.07	43	2.0
9	0.025	21	0.01	32	0.08	44	4.0
10	0.025	22	0.008	33	0.1	45	8.0
11	0.025	23	0.006	34	0.1	46	16.0
12	0.02	24	0.004	35	0.13		
Mesh 2.2							
i	h_i	i	h_i	i	h_i	i	h_i
1	0.05	4	0.15	7	0.2	9	0.01
2	0.1	5	0.2	contact		10	0.02
3	0.1	6	0.2	8	0.005		
j	w_j	j	w_j	j	w_j	j	w_j
1	0.1	7	0.03	12	0.15	18	1.0
2	0.1	8	0.02	13	0.2	19	2.0
3	0.08	9	0.01	14	0.3	20	4.0
4	0.07	contact		15	0.4	21	8.0
5	0.05	10	0.05	16	0.55	22	16.0
6	0.04	11	0.1	17	0.75		
Mesh 2.3							
i	h_i	i	h_i	i	h_i	i	h_i
1	0.2	4	0.2	contact		7	0.01
2	0.2	5	0.2	6	0.005	8	0.02
3	0.2						
j	w_j	j	w_j	j	w_j	j	w_j
same as Mesh 2.2							

Table 5
Comparison of amplitude data for Example 2. The difference between each datum and the corresponding Mesh 2.1 datum is in parentheses

<i>y</i> (km)	Log ₁₀ Amplitude			
	Mesh 2.1	Mesh 2.2 MOM	Mesh 2.2 Std	Mesh 2.3 MOM
0.0	1.859	1.854 (-0.005)	1.912 (0.053)	1.850 (-0.009)
0.1	1.882	1.878 (-0.004)	1.938 (0.056)	1.873 (-0.009)
0.2	1.961	1.955 (-0.006)	2.021 (0.060)	1.948 (-0.013)
0.25	2.028	2.028 (0.0)	2.099 (0.071)	2.018 (-0.010)
0.3	2.122	2.122 (0.0)	2.200 (0.078)	2.108 (-0.014)
0.35	2.261	2.252 (-0.009)	2.343 (0.082)	2.231 (-0.030)
0.4	2.476	2.466 (-0.010)	2.579 (0.103)	2.423 (-0.053)
0.425	2.642	2.636 (-0.006)	2.771 (0.129)	2.562 (-0.080)
0.45	2.886	2.876 (-0.010)	3.047 (0.161)	2.748 (-0.138)
0.46	3.026	3.015 (-0.011)	3.209 (0.183)	2.849 (-0.177)
0.47	3.205	3.180 (-0.025)	3.408 (0.203)	2.963 (-0.242)
0.48	3.469	3.413 (-0.056)	3.734 (0.265)	3.042 (-0.427)
0.49	3.934	3.731 (-0.203)	4.261 (0.327)	3.129 (-0.805)
0.495	4.386	4.312 (-0.074)	4.825 (0.439)	3.721 (-0.665)
0.5-	6.935	6.941 (0.006)	6.960 (0.025)	6.957 (0.022)
0.5+	0.527	0.533 (0.006)	0.552 (0.025)	0.549 (0.022)
0.51	0.543	0.543 (0.0)	0.562 (0.019)	0.558 (0.015)
0.55	0.584	0.587 (0.003)	0.603 (0.019)	0.597 (0.013)
0.6	0.624	0.622 (-0.002)	0.637 (0.013)	0.628 (0.004)
1.0	0.801	0.802 (0.001)	0.820 (0.019)	0.803 (0.002)
2.0	0.953	0.949 (-0.004)	0.970 (0.017)	0.949 (-0.004)
10.0	0.994	0.993 (-0.001)	1.015 (0.021)	0.993 (-0.001)
34.0	0.994	0.993 (-0.001)	1.015 (0.021)	0.993 (-0.001)
				Mesh 2.3 Std
				2.082 (0.223)
				2.110 (0.228)
				2.205 (0.244)
				2.294 (0.266)
				2.410 (0.288)
				2.575 (0.314)
				2.844 (0.368)
				3.058 (0.416)
				3.362 (0.476)
				3.537 (0.511)
				3.756 (0.551)
				4.089 (0.620)
				4.637 (0.703)
				5.186 (0.800)
				7.038 (0.103)
				0.630 (0.103)
				0.637 (0.094)
				0.668 (0.084)
				0.699 (0.075)
				0.879 (0.078)
				1.037 (0.084)
				1.085 (0.091)
				1.085 (0.091)

Table 6

Element dimensions for Meshes 3.1 and 3.2 used in Example 3.

Mesh 3.1							
<i>i</i>	<i>h_i</i>	<i>i</i>	<i>h_i</i>	<i>i</i>	<i>h_i</i>	<i>i</i>	<i>h_i</i>
1	256.0	10	0.7	18	1.6	27	12.8
2	128.0	11	0.5	19	2.0	28	16.0
3	64.0	12	0.3	20	2.6	29	32.0
4	32.0	contact		21	3.2	30	64.0
5	16.0	13	0.3	22	4.0	31	128.0
6	8.0	14	0.5	23	5.2	32	128.0
7	4.0	15	0.7	24	6.4	contact	
8	2.0	16	1.0	25	8.0	33	128.0
9	1.0	17	1.3	26	10.4		
<i>j</i>	<i>w_j</i>	<i>j</i>	<i>w_j</i>	<i>j</i>	<i>w_j</i>	<i>j</i>	<i>w_j</i>
1	160.0	8	8.0	contact		21	2.6
2	80.0	9	6.0	15	0.3	22	4.0
3	40.0	10	4.0	16	0.4	23	8.0
4	26.0	11	3.0	17	0.6	24	16.0
5	18.0	12	2.5	18	0.9	25	32.0
6	14.0	13	1.5	19	1.4	26	64.0
7	11.0	14	1.0	20	1.8		
Mesh 3.2							
<i>i</i>	<i>h_i</i>	<i>i</i>	<i>h_i</i>	<i>i</i>	<i>h_i</i>	<i>i</i>	<i>h_i</i>
1	258.5	7	4.0	12	4.0	18	32.0
2	128.0	8	2.0	13	8.0	19	64.0
3	64.0	contact		14	8.0	20	128.0
4	32.0	9	2.0	15	16.0	21	128.0
5	16.0	10	2.0	16	16.0	contact	
6	8.0	11	4.0	17	16.0	22	128.0
<i>j</i>	<i>w_j</i>	<i>j</i>	<i>w_j</i>	<i>j</i>	<i>w_j</i>	<i>j</i>	<i>w_j</i>
1	160.0	6	20.0	10	1.0	15	8.0
2	80.0	7	10.0	11	2.0	16	16.0
3	40.0	8	10.0	12	2.0	17	32.0
4	30.0	9	5.0	13	3.0	18	64.0
5	20.0	contact		14	4.0		

0.9947. Meshes 2.2 and 2.3, which differ only in their vertical node spacings, are considerably less detailed. Phase data were not used in this example.

Table 5 shows that MOM's method produces consistently better results than the standard method. The errors using MOM's method are large only over the dyke near $y = 0.5$ km. In this region the element widths of Meshes 2.2 and 2.3 are too large to represent the rapidly varying E_y field caused by the large conductivity contrast of 1600 : 1.

Example 3: E_x mode over vertical contact

Meshes 3.1 and 3.2, described in Table 6, were used to solve the E_x mode over the vertical contact in Fig. 3. Mesh 3.1 is more detailed and its data were taken to be very accurate. Therefore, the errors in the Mesh 3.2 results are with respect to the Mesh 3.1 data.

The standard method results were obtained using g_9^- rather than g_9^+ ; the numerical differentiation was done using the surface nodes and the first row of nodes above the surface. In MOM's method, $g_9^+ = g_9^-$.

Table 7 shows that MOM's method again is more accurate (with exceptions) than the standard method, but not dramatically as in Example 1. One reason for this is that the E_x mode over a structure with lateral conductivity, but no lateral per-

Table 7

Comparison of amplitude and phase data for Example 3. Differences between Mesh 3.2 data and Mesh 3.1 data are in parentheses.

y (km)	Log_{10} Amplitude		
	Mesh 3.1	Mesh 3.2 MOM	Mesh 3.2 Std
-100	-2.013	-2.013 (0.0)	-2.012 (0.001)
-50	-1.970	-1.968 (0.002)	-1.964 (0.006)
-40	-1.930	-1.925 (0.005)	-1.918 (0.012)
-30	-1.861	-1.855 (0.006)	-1.845 (0.016)
-20	-1.733	-1.730 (0.003)	-1.716 (0.017)
-15	-1.621	-1.635 (-0.014)	-1.618 (0.003)
-10	-1.453	-1.431 (0.022)	-1.403 (0.050)
-5	-1.176	-1.204 (-0.028)	-1.166 (0.010)
-2	-0.885	-0.836 (0.049)	-0.817 (0.068)
0	-0.563	-0.602 (-0.039)	-0.593 (-0.030)
1	-0.377	-0.358 (0.019)	-0.443 (-0.066)
2	-0.276	-0.281 (-0.005)	-0.349 (-0.073)
3	-0.205	-0.201 (0.004)	-0.254 (-0.049)
5	-0.102	-0.095 (0.007)	-0.137 (-0.035)
10	0.005	0.008 (0.003)	-0.009 (-0.014)
15	0.019	0.023 (0.004)	0.017 (-0.002)
20	0.008	0.011 (0.003)	0.012 (0.004)
30	0.004	0.008 (0.004)	0.008 (0.004)
40	0.001	0.005 (0.004)	0.005 (0.004)
50	0.002	0.006 (0.004)	0.006 (0.004)

y (km)	Phase (degrees)		
	Mesh 3.1	Mesh 3.2 MOM	Mesh 3.2 Std
-100	3.9	3.7 (-0.2)	3.8 (-0.1)
-50	15.7	15.7 (0.0)	16.0 (0.3)
-40	20.6	20.6 (0.0)	20.9 (0.3)
-30	26.8	26.8 (0.0)	27.1 (0.3)
-20	34.1	33.9 (-0.2)	34.1 (0.0)
-15	37.7	37.6 (-0.1)	37.7 (0.0)
-10	40.1	39.7 (-0.4)	38.5 (-1.6)
-5	37.3	39.6 (2.3)	37.2 (-0.1)
-2	25.1	19.3 (-5.8)	17.8 (-7.3)
0	1.0	4.5 (3.5)	3.3 (2.3)
1	-12.4	-15.9 (-3.5)	-8.7 (3.7)
2	-16.4	-17.0 (-0.6)	-12.7 (3.7)
3	-17.5	-19.0 (-1.5)	-17.6 (-0.1)
5	-17.1	-18.7 (-1.6)	-18.6 (-1.5)
10	-9.0	-10.3 (-1.3)	-11.6 (-2.6)
15	-3.2	-4.6 (-1.4)	-5.6 (-2.4)
20	0.3	-1.0 (-1.3)	-1.4 (-1.7)
30	-0.1	-1.4 (-1.3)	-1.6 (-1.7)
40	-0.4	-1.7 (-1.3)	-1.7 (-1.3)
50	-0.3	-1.6 (-1.3)	-1.6 (-1.3)

meability, changes is an easier problem to solve than the H_x mode. Another reason is that using the air layer to numerically differentiate removes part of the need for MOM's method. This is easily seen in the one-dimensional case, where in (5.11) $\gamma = 0$ in air for the E_x mode. In the two-dimensional case, (2.1) implies

$$\partial_x J = -\gamma V + \partial_y((1/\eta)\partial_y V). \quad (8.1)$$

MOM's method adds in a z dependence for J . When $\gamma = 0$, the z dependence is caused only by a second derivative of V . So MOM's method and the standard method are less different in the E_x mode than in the H_x mode, where $\gamma \neq 0$.

9. Conclusions

The definition of J in (5.3) and (5.6) and MOM's algorithm for computing J comprise a straightforward extension of a basically simple FE method and significantly enhance the accuracy of the method in MT modelling. This is particularly valuable in implementing linear inverse methods, where efficiency is important and meshes of marginal quality are likely to be encountered.

The primary accomplishment of MOM's method is that it allows the auxiliary field J to have the same functional dependence on y and z as the solution field V . It does this in a way that is consistent with the FE procedure for incorporating boundary conditions into the Lagrangian.

The method corrects mainly for insufficient vertical node spacing and has less effect on insufficient horizontal node spacing. However, this does not mean that MOM's method is only appropriate for regions where the solution field is one-dimensional. It is most accurate in one-dimensional regions simply because horizontal node spacing has no effect when the solution depends only on depth.

Finally, MOM's method is more helpful in the H_x mode than the E_x mode because in the E_x mode the combined effects of $\sigma = 0$ in air and $\mu = 4\pi \times 10^{-7}$ everywhere result in a relatively slow variation of H_y with z in air.

Acknowledgments

This work was supported by the National Science Foundation under Grant GA 38731 and The Pennsylvania State University Computation Centre. The author is grateful to Dr R. J. Greenfield for his helpful comments about the manuscript.

*Department of Geosciences
The Pennsylvania State University
University Park, Pennsylvania 16802*

References

- Backus, G. E. & Gilbert, J. F., 1967. Numerical applications of a formalism for geophysical inverse problems, *Geophys. J. R. astr. Soc.*, **13**, 247–276.
- Coggon, J. H., 1971. Electromagnetic and electrical modeling by the finite element method, *Geophysics*, **36**, 132–155.
- d'Erceville, I. & Kunetz, G., 1962. The effect of a fault on the Earth's natural electromagnetic field, *Geophysics*, **27**, 651–665.
- Jones, F. W. & Pascoe, L. J., 1971. A general computer program to determine the perturbation of alternating electric currents in a two-dimensional model of a region of uniform conductivity with an embedded inhomogeneity, *Geophys. J. R. astr. Soc.*, **24**, 3–30.
- Jones, F. W. & Thomson, D. J., 1974. A discussion of the finite difference method in computer modelling of electrical conductivity structures. A reply to the discussion by Williamson, Hewlett and Tammemagi, *Geophys. J. R. astr. Soc.*, **37**, 537–544.
- Jordan, T. H., 1973. *Estimation of the radial variation of seismic velocities and density in the Earth*, PhD Thesis, California Institute of Technology.
- Madden, T. R., 1972. Transmission systems and network analogies to geophysical forward and inverse problems, *Technical Report N000-14-67-A-0204-0045, M.I.T. Report No. 72-3*, Dept. of Earth and Planetary Sciences, Massachusetts Institute of Technology.
- Morse, P. M. & Feshbach, H., 1953. *Methods of theoretical physics*, McGraw-Hill, New York.

- Pascoe, L. J. & Jones, F. W., 1972. Boundary conditions and calculation of surface values for the general two-dimensional electromagnetic induction problem, *Geophys. J. R. astr. Soc.*, **27**, 179–193.
- Rankin, D., 1962. The magnetotelluric effect on a dyke, *Geophysics*, **27**, 666–676.
- Reddy, I. K. & Rankin, D., 1973. Magnetotelluric response of a two-dimensional sloping contact by the finite element method, *Pure appl. Geophys.*, **105**, 847–857.
- Silvester, P. & Haslam, C. R. S., 1972. Magnetotelluric modelling by the finite element method, *Geophys. Prospect.*, **20**, 872–891.
- Swift, C. M., 1967. *A magnetotelluric investigation of an electrical conductivity anomaly in the southwestern United States*, Ph.D Thesis, Massachusetts Institute of Technology.
- Williamson, K., Hewlett, C. & Tammemagi, H. Y., 1974. Computer modelling of electrical conductivity structures, *Geophys. J. R. astr. Soc.*, **37**, 533–536.
- Zienkiewicz, O. C., 1971. *The finite element method in engineering science*, McGraw-Hill, New York.